Kinetics and wavelength dependence of thermal and gain lens induced in Nd:YAG rod amplifier

Martin Maillard, Gabriel Amiard-Hudebine, Marc Tondusson, Mikael Orain, Eric Freysz

Important Notice to Authors

Attached is a PDF proof of your forthcoming article in Optics Express. The article Manuscript ID is 478909. *No further processing of your paper will occur until we receive your response to this proof.*

Note: *Excessive proof corrections submitted by the author can result in significant delays to publication. Please include only essential changes that might be needed to address any shortcomings noticed in the proof-preparation process.*

Author Queries

Please answer these queries by marking the required corrections at the appropriate point in the text or referring to the relevant line number in your PDF proof.

Q1	The funding information for this article has been generated using the information you provided to us at the time of article submission. Please check it carefully. If any information needs to be corrected or added, please provide the full name of the funding organization/institution as provided in the Crossref Open Funder Registry (https://search.crossref.org/funding).

Other Items to Check

- Please note that the original manuscript has been converted to XML prior to the creation of the PDF proof, as described above. The PDF proof was generated using LaTeX for typesetting. The placement of your figures and tables may not be identical to your original paper.
- Please carefully check all key elements of the paper, particularly the equations and tabular data.
- Author list: Please make sure all authors are presented, in the appropriate order, and that all names are spelled correctly.
- If you need to supply new or replacement figures, please upload each figure as an individual PDF file at the desired final figure size. The figure must fit inside the margins of the manuscript, i.e., width no more than 5.3 inches (or 13.46 cm). Confirm the quality of the figures and upload the revised files when submitting proof corrections.

Research Article | Vol. 0, No. 0 / 00 00 0000 / Optics Express 1

Optics EXPRESS

Kinetics and wavelength dependence of thermal and excited-state population lensing effect induced in a Nd:YAG rod amplifier

MARTIN MAILLARD,[1,2] GABRIEL AMIARD-HUDEBINE,[2] MARC TONDUSSON,[2] MIKAËL ORAIN,[1] AND ERIC FREYSZ[2,*]

[1] ONERA/DMPE, Université de Toulouse, 31055 Toulouse, France
[2] University of Bordeaux, CNRS, LOMA, UMR 5798, F-33400 Talence, France
[*] eric.freysz@u-bordeaux.fr

Abstract: Using a wavefront sensor, we have measured the temporal evolution of the lens induced in a Nd:YAG rod amplifier under side pumping by laser diode bars centered around 808 nm in a quasi-continuous wave regime. The evolution of the induced lens is drastically different when measured with a probe pulse centered at 532 nm or 1064.5 nm. To explain this evolution, we developed a model that accounts for both the excited state population of the Nd^{3+} ions and the thermal contribution to the refractive index of the amplifier. This model, which takes into account amplification and wavelength shift of the probe pulse at 1064.5 nm, makes it possible to quantitatively describe the spectral and temporal evolution of the amplifier focal length. It also shows that the excited state population contribution is more important around 1064.5 nm and can partly compensate for the thermal lens induced in the amplifier.

1. Introduction

Master oscillator and power amplifier (MOPA) have attracted a lot of attention in recent years [1–6]. When high power is required, MOPA performs well compared with simple laser oscillator in terms of linewidth, wavelength tuning range, beam quality and pulse duration. To master the design of a MOPA, it is of crucial importance to evaluate and control the impact of the different amplification stages on the initial spatial beam profile. While the master oscillator can easily delivers laser pulses with a very good gaussian beam shape ($M^2 \leq 1.2$), power amplifier usually degrades the beam quality. The latter mainly results from an index gradient established perpendicularly to the propagation axis of the laser beam within the amplifying medium (AM). This index gradient is mainly due to the thermal gradient induced during the optical pumping of the AM. In a first approximation, this thermal gradient has generally a parabolic shape and the AM acts as a lens. This thermal lens often degrades the amplified beam profile, and in the worst case, it can damage the AM. The focal length of the thermal lens depends on the amplitude and shape of refractive index change (RIC) induced during the optical pumping of the AM. It writes $1/f_T \propto \frac{\delta n'(\lambda)}{\delta T} \nabla_r T$ where $\nabla_r T$ is the spatial thermal gradient and $\frac{\delta n'(\lambda)}{\delta T}$ is the thermal variation of the refractive index at laser wavelength λ [7], which depends on the density and the polarizability of the AM [8]. The thermal gradient further generates deformations and stresses which modifies the focal length f_T of the AM [9]. To improve the beam quality delivered by oscillators and laser amplifiers, different studies have reported the thermal lens in the AM [1,9–12]. It is worth mentioning that the heat equation drives the temporal evolution of the thermal lens effect in the AM.

However, besides thermal lens effect, another phenomenon also happens during the optical pumping of the amplifiers. This phenomenon, often overlooked, is linked to the change of the AM complex refractive index $n(\lambda) = n'(\lambda) + in''(\lambda)$ during the population of the different electronic states of the doping ions [13–17]. As for the thermal effect and during the AM

#478909 https://doi.org/10.1364/OE.478909
Journal © 0000 Received 24 Oct 2022; revised 2 Dec 2022; accepted 4 Dec 2022; published 00 00 0000

Optics EXPRESS

optical pumping, a spatial gradient of the density of excited state population $\nabla_r N_{ex}$ is established perpendicularly to the propagation axis of the amplified pulse. It also results in a spatial gradient of refractive index which makes the AM behave like a lens. The associated focal length writes: $1/f_{N_{ex}} \propto \frac{\delta n'(\lambda)}{\delta N_{ex}} \nabla_r N_{ex}$, where $\nabla_r N_{ex}$ is the spatial population gradient and $\frac{\delta n'(\lambda)}{\delta N_{ex}}$ is the population variation of the refractive index at laser wavelength λ. At variance with the thermal lens effect, the kinetic of this latter phenomenon is driven by the population and the relaxation time of N_{ex}. It was found to dominate over the thermal effects in Yb-doped crystals and glasses under pulse pumping [18–20]. It is comparable with the thermal effect in Nd-doped materials [21–24]. Hereafter, using a wavefront analysis method, we show that excited state population and thermal lenses can be easily revealed in a Nd:YAG rod amplifier under quasi-continuous side pumping by laser diode bars centered around 808 nm. Our technique makes it possible to record the temporal evolution of a probe pulse wavefront propagating in the AM. It is easily operated at various wavelengths, thanks to the broadband absorption spectra of the wavefront analyzer. Knowing the evolution of the curvature radius of this probe beam, we can quantitatively infer the evolution of the lens induced in the AM. In order to analyze our experimental results, we developed a model which accounts for the refractive index change (RIC) of the AM induced by both excited state population and thermal effects. We show that in our Nd:YAG rod amplifier, the excited state population contribution is more important at 1064 nm and can partly compensate for the thermal lens.

2. Experimental setup

We use the setup displayed in Fig. 1(a). It measures the temporal evolution of the radius of curvature (ROC) of the probe beam at the exit of AM using a Schack-Hartmann wavefront sensor (WFS). This WFS (Thorlabs WFS40-5C), built around a 2048 x 2048 pixels CMOS camera, has an array of 73 x 73 microlens array. According to the deviation of each microlens beam spot, compared to the plane wave spot position, one can recalculate the local angle of incidence. The latter makes it possible to record the beam phase and to infer the ROC of the probe beam. Our WFS is able to measure the change of the ROC between 0.005 m and 100 m on a large spectral range (300 nm to 1100 nm). The AM used in this work, is 3 mm in diameter and 70 mm long Nd:YAG rod (Northrop Grumman RBAT34-1C2). It is side pumped by quasi-continuous-wave (QCW) optical pulses delivered by laser diode bars having central wavelength around 808 nm. Figure 1(b), represents the spectrum of spontaneous emission of the AM upon QCW excitation. A Nd:YAG microlaser (Standa STA-01-7-OEM) delivers the probe beam at a frequency of 100 Hz. The probe pulse has a duration of $\sim$ 700 ps, an energy of $\sim$ 200 µJ and it has a good Gaussian beam shape ($M^2 \leq 1.3$). Figure 1(b) displays its spectrum. It is worth noting that its central wavelength is 1064.5 nm, slightly shifted from the main emission peak of the Nd:YAG at 1064.2 nm [25]. We send the linearly polarized probe pulse through a half-wave plate placed in front of a Faraday isolator. Afterward, it propagates through a half wave-plate and a polarizing beam splitter to finely adjust the energy of the pulse propagating in the AM. We measure the change of the ROC of the probe beam when it is either amplified (1064.5 nm) and non amplified (532 nm). To perform the experiment at 532 nm, we focus the probe beam and frequency double it in a BBO crystal, then a lens colimates it.

To provide reliable measurements of the ROC, we ensure that the beam size of the probe pulse remains constant on the WFS and that the spot size covers the whole CMOS sensor. In order to satisfy these two requirements, we conjugate the exit of the AM with the WFS using a pair of lenses (L_3 and L_4). As the size of the beam at the exit of the AM changes at 1064.5 nm and 532 nm, two different sets of lenses are used. Prior to our experiments, we measured the initial ROC of the probe beam reflected by the polarizing beam splitter and collected by a removable mirror. To check the magnification G of our conjugation system , we inserted a set of lenses with known focal length f_{cal} with value between 50 and 2000 mm in the optical path of beam reflected

Optics EXPRESS

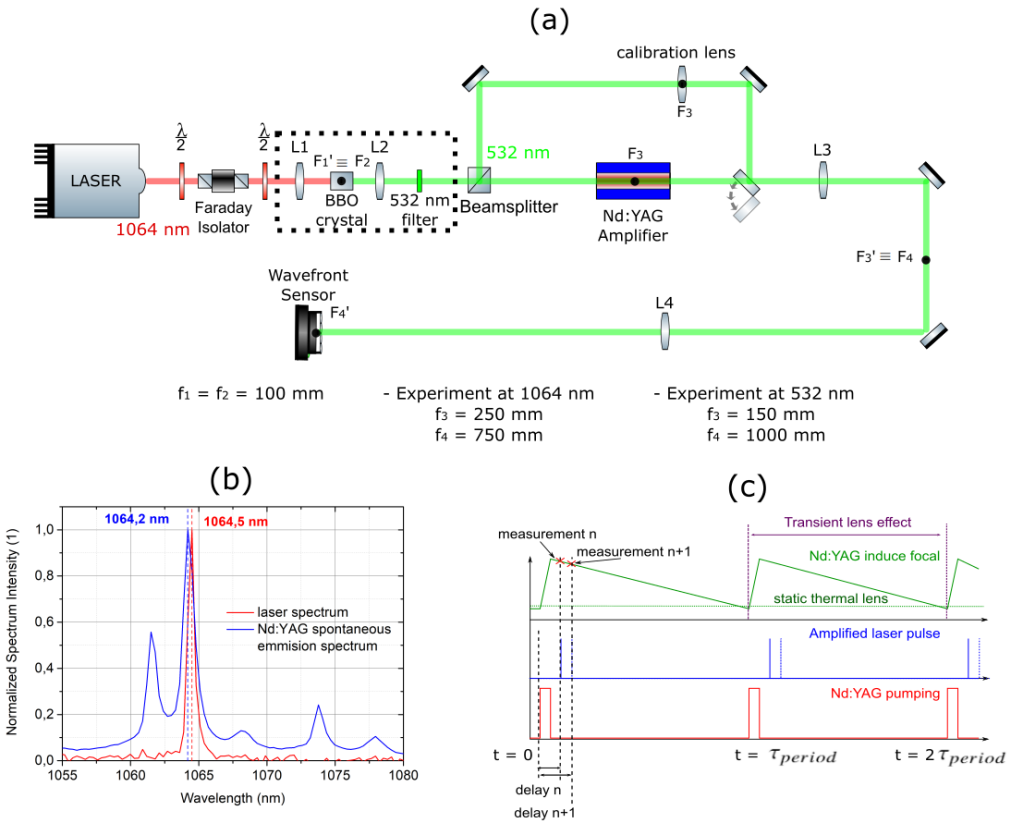

Fig. 1. (a) Experimental setup used to measure the temporal evolution of the focusing effect induced by AM pumping. (b) Spectrum of the laser source (red curve) and of the AM spontaneous emission (blue curve). (c) Chronogram of the different events of the experiment.

by the beam splitter. Therefore, we were able to plot the ROC as a function of the focal length and so accurately calculate the magnification $G = f_4/f_3$ of our optical conjugation system. The ROC recorded by our WFS is directly linked to f_{cal} and writes: $ROC = G^2 f_{cal}$. The linear fits of these ROCs indicate the measured magnifications $G^m_{1064\,\mathrm{nm}} = 3.08 \pm 0.10$ and $G^m_{532\,\mathrm{nm}} = 6.63 \pm 0.05$ at 1064.5 nm and 532 nm, respectively. The values are in good agreement with the focal length of the lenses L_3 and L_4 for which $G^e_{1064\,\mathrm{nm}} = 3$ and $G^e_{532\,\mathrm{nm}} = 6,67$ (Fig. 1(a)). We record the temporal evolution of the ROC upon optical excitation of the AM as follow. We synchronize the pulse delivered by the microlaser with the power supply controlling the laser diodes bars. Then, by delaying in time the electrical and microlaser pulses (Fig. 1(c)), we measure the temporal evolution of the ROC of the probe beam at the exit of the AM. The power supply of the laser diode is able to deliver electrical pulses of duration up to 600 µs and current up to 100 A at 100 Hz.

3. Experimental results

The temporal evolution of the focal lens $f(t)$ induced in the AM upon its excitation is directly related to the temporal evolution of the probe beam radius of curvature $ROC(t)$ at the exit of the AM. It writes $f(t) = ROC(t)/G^2$ where G is the magnification of our conjugation system.

Optics EXPRESS

3.1. Evolution of the focal length of the AM recorded at $\lambda = 1064.5\ nm$

Figure 2 displays the temporal evolution of the gain (Fig. 2(a)) and the focal length (Fig. 2(b)) of the AM upon its optical excitation. We record these data, driving the pump diodes with current of 100 A and a duration of 500 µs. As expected, during the excitation of the AM, the gain g increases up to $g \sim 13$ at the end of the pump pulse. It then steadily relaxes back to $g = 1$. When the pump pulse is on, the focal length f of the AM starts from its quasi steady state regime value $f_{qs} = 0.53 \pm 0.02$ m and rapidly increases up to $f = 0.61 \pm 0.02$ m after $\sim$ 150 µs. Afterward, it decreases to $f = 0.53 \pm 0.02$ m at the end of the pump pulse. As soon as the pump pulse is off, the focal length of the AM increases again and it is $f = 0.60 \pm 0.02$ m after about 250 µs. Afterward, it relaxes back to its quasi-static value f_{qs}. We also record the evolution of the focal length of the AM while changing the current and the duration of the pump pulse. As displayed in Fig. 3(a), when the current I increases, f_{qs} decreases. It is $f_{qs} = 0.78 \pm 0.03$ m for $I = 80$ A and $f_{qs} = 0.52 \pm 0.02$ m for $I = 100$ A. It is worth noticing that whatever the current, the focal length $f(t)$ of the AM is maximum after about 150 µs and then decreases. Similarly, when the pump current I is off, $f(t)$ increases and reaches its maximum 250 µs later and then decreases back. The same trend is observed while keeping the current I constant but increasing the duration of the pump pulse from 400 µs to 600 µs (Fig. 3(b)).

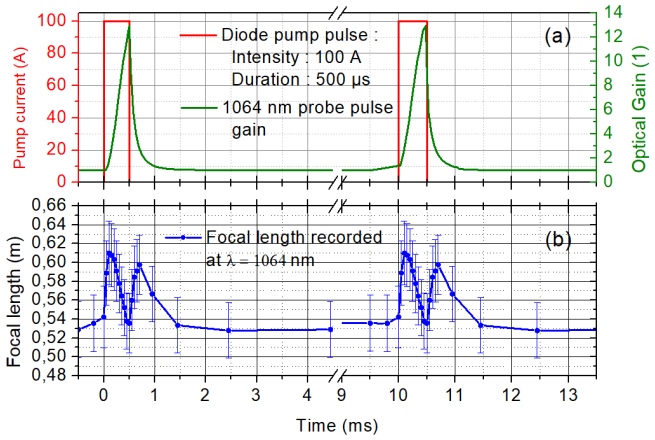

Fig. 2. (a) Temporal shape of the 500 µs laser diode electrical pulses (red curve). Evolution of the gain in the Nd:YAG rod for the probe pulse centered at $\lambda = 1064,5$ nm (green curve). (b) Temporal evolution of the focal length $f(t)$ induced in the Nd:YAG rod recorded with a probe pulse centered at $\lambda = 1064,5$ nm.

3.2. Evolution of the focal length of the AM recorded at $\lambda = 532\ nm$

We also record the focal length of the Nd:YAG rod at $\lambda = 532$ nm. For this experiment, due to an electrical problem that overheated the pump diode, its central wavelength shifted from 808 nm to 803.7 nm. The absorption coefficient of the AM at this wavelength is slightly lower. The evolution of the focal length of the AM recorded at $\lambda = 532$ nm is displayed in Fig. 4(b) when a current of 100 A is applied during $\tau_{pump} = 500$ µs at a repetition rate of 100 Hz to the laser diode bars. Under this condition, the quasi static focal length of the AM is $f_{qs} = 0.74 \pm 0.02$ m. At variance with the experiment operated at $\lambda = 1064.5$ nm, when the pump is on, the focal length $f(t)$ of the AM always decreases. At the end of diode pump pulse, it is about $f(500\ \mu s) = 0.68 \pm 0.02$ m. When the pump is off , $f(t)$ slowly increases back to its quasi-steady value. The increase of the focal length of the AM can be fitted by a sum of two increasing exponential functions, highlighting two characteristic times $\tau_1 = 236 \pm 10$ µs and $\tau_2 = 8.0 \pm 0.2$ ms. The result of this fit is plotted

Optics EXPRESS

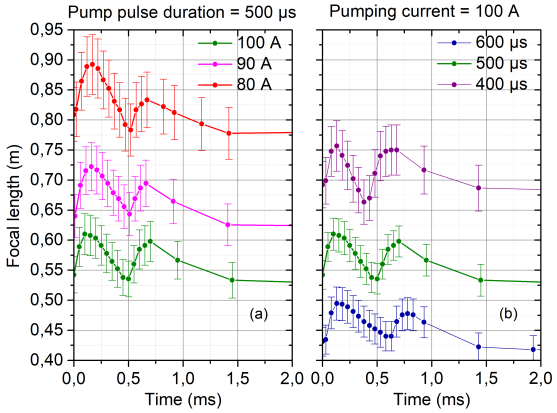

Fig. 3. Temporal evolution of the focal length $f(t)$ of the Nd:YAG rod recorded with a probe pulse centered at $\lambda = 1064.5$ nm. The evolution of focal length $f(t)$ is plotted when the Nd:YAG rod is excited by laser diode bars (a) a duration of 500 µs with different diode pump currents, (b) with different pulse durations and a fixed current of 100 A.

in red dash in Fig. 4(b). As discussed later, τ_1 corresponds to the relaxation time of excited Nd^{3+} ions in the YAG matrix and τ_2 is related to the diffusion of heat within the Nd:YAG rod. This phenomenon was already observed by Antipov [13].

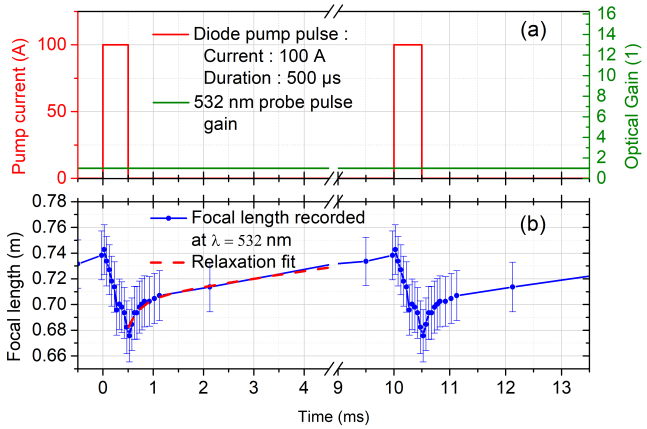

Fig. 4. (a) Temporal evolution of the laser diode electrical pulses, for a current of 100 A and 500 µs duration (red curve), and evolution of the laser probe gain when the its central wavelength is at $\lambda = 532$ nm (green curve). (b) Evolution of the focal length of the Nd:YAG rod at $\lambda = 532$ nm (blue dots). The red dashed line displays the relaxation of f back to its quasi-steady state value f_{qs}.

4. Modification of the refractive index of the Nd:YAG rod induced by the thermal process

As already mentioned, the optical excitation of the Nd^{3+} ions in the YAG matrix increases the temperature of the AM which in turn modifies its refractive index. This is due to the quantum defect $\eta_h \sim 24\%$ of the AM induced by the difference in energy between the photon absorbed (around 808 nm) and emitted (around 1064 nm) by the Nd^{3+} ions (see Fig. 1(b)). The RIC δn_T

Optics EXPRESS

induced by temperature variation writes [7]:

$$\delta n_T = \left(\frac{dn}{dT}\right)_{eff} \Delta T, \tag{1}$$

where $\left(\frac{dn}{dT}\right)_{eff}$ is the effective thermo-optic coefficient. This coefficient accounts for the thermo-optic effect, the photo-elastic deformation, the stress and strain effects [14]. To model our experiment, we will consider that the radius R of our Nd:YAG rod is small compared to its length L ($R \ll L$) and behaves as an infinite cylinder. The temporal and spatial evolution of the temperature within the Nd:YAG rod can be computed by solving the heat equation. In cylindrical coordinates, the latter writes:

$$K_c \nabla^2 T + Q(r,t) = \rho C_p \frac{\partial T}{\partial t}, \tag{2}$$

where $Q(r,t)$ is the source of heat, K_c the thermal conductivity, ρ the density and C_p the specific heat capacity of the YAG, r is the radial coordinate and t the time. This equation has to be supplemented by the boundaries conditions. The YAG rod being side-cooled by water, we assume that at its edge $T(r = R; t) = 298$ K. We also consider that prior to its optical pumping, the Nd:YAG rod is at ambient temperature ($T(r; t = 0) = 298$ K). The temporal and spatial profile of the temperature within the Nd:YAG rod strongly depends on the way heat is deposited in the AM. The Nd:YAG rod is side pumped and the pump absorption within the rod has almost a Gaussian shape. Hence, the heat source writes:

$$Q(r,t) = Q_0(t) e^{-\frac{r^2}{2.\sigma_{pump}^2}}, \tag{3}$$

where σ_{pump} is the pump cross section and $Q_0(t) = Q(r = 0, t)$. The evolution of $Q_0(t)$ is driven by the number of Nd^{3+} ions excited in the $^4F_{3/2}$ level. When the pump intensity is small compared to the saturation intensity, the excited state population equation writes [26]:

$$N_{ex}(t) = N_0 \left(1 - e^{-\frac{R^2}{2\sigma_{pump}^2}}\right) \begin{cases} 1 - e^{-\frac{t}{\tau}} & \text{if } t<\tau_{pump} \\ \left(1 - e^{-\frac{\tau_{pump}}{\tau}}\right) e^{-\frac{t-\tau_{pump}}{\tau}} & \text{if } \tau_{pump}<t<\tau_{period} \end{cases}, \tag{4}$$

where $\tau_{pump}, \tau_{period}, \tau, N_0$ are the pump pulse duration, the pumping period (10 ms), the relaxation time of the $^4F_{3/2}$ level ($\tau = 230$ µs) and the concentration of excited Nd^{3+} ions, respectively. The latter parameter writes:

$$N_0 = \eta_{abs} N_{tot}, \tag{5}$$

where η_{abs} and N_{tot} are the AM pump absorption efficiency and the Nd^{3+} doping concentration, respectively. The heat generated within the AM is depending if it is pumped or not. During the pumping, we consider the heat source results from the Nd^{3+} quantum defect which is $\eta_h \sim 24\%$. It is due to the non-radiative relaxation from the $^4F_{5/2}$ to the $^4F_{3/2}$ and from the $^4I_{11/2}$ to the $^4I_{9/2}$ ($\eta_h^{10} = 13\%$). It is worth noting that under our non-lasing condition, the undesirable thermal load of the AM which can be increasing up to 38% by the population of the $^4F_{3/2}$ is considerably reduced due to our low pump duty cycle [27]. This phenomenon is neglected hereafter. Hence, the heat source writes:

$$Q(r,t) = \frac{N_0 hc}{\lambda_{pump} \tau_{period}} e^{-\frac{r^2}{2\sigma_{pump}^2}} \left(1 - e^{-\frac{R^2}{2\sigma_{pump}^2}}\right) h(t) \tag{6}$$

Optics EXPRESS

with

$$h(t) = \begin{cases} \eta_h(1 - e^{-\frac{t}{\tau}}) & \text{if } t<\tau_{pump} \\ \eta_h^{10}\left(1 - e^{-\frac{\tau_{pump}}{\tau}}\right) e^{-\frac{t-\tau_{pump}}{\tau}} & \text{if } \tau_{pump}<t<\tau_{period} \end{cases}, \quad (7)$$

where h, c, λ_{pump} are the Planck's constant, the speed of light in vacuum and the pump wavelength, respectively.

To solve the heat equation (Eq. (2)), we used the multiphysics software COMSOL. All the parameters used in the simulations are summarized in Table 1. The results of our simulations, computed considering that the AM is excited at a repetition rate of 100 Hz by a pump pulse of 500 µs centered at λ_{pump} = 808 nm (for the experiment at 1064 nm) or λ_{pump} = 803.7 nm (for the experiment at 532 nm), are displayed in Fig. 5. It is important to mention that when the pump is switched on for the first time, the whole temperature of the Nd:YAG rod increases during ~ 4 s before reaching this quasi-steady state regime (QSSR). Afterwards, the temperature gradient inside the rod periodically evolves as displayed in this figure. The evolution of the heat $Q_0(t)$ generated within the Nd:YAG rod and the temperature difference $\Delta T(t)$ between the center and the edge of the Nd:YAG rod in the QSSR are displayed in Fig. 5(a) in red and blue, respectively. In this QSSR, one can write:

$$\Delta T(t) = \Delta T_{QSSR} + \delta T(t). \quad (8)$$

According to the data displayed in Fig. 5(a), $\Delta T_{QSSR} \sim 4K$ and $\delta T(t) \leq 0.10$ K. It is worth noting that in this QSSR, $\delta T(t)$ increases during ~ 1 ms even if the pump pulse lasts only 500 µs. Indeed when we switch the pump off, heat is still generated within the AM due to the relaxation of N_{ex}. According to Eq. (1), the RIC adopts the temporal distribution of $\Delta T(t)$ (Fig. 5(b)). In Fig. 5(c), we plotted the temperature distribution $T_{QSSR}(r)$ along the diameter of the Nd:YAG rod. This radial distribution is well fitted by a second order polynomial and properly accounts for the occurrence of a thermal lens. The thermal focal length induced by this temperature gradient writes [7]:

$$f_T = -\frac{1}{2L\left(\frac{\partial^2 n(r)}{\partial r^2}\right)_{r=0}}, \quad (9)$$

where,

$$\frac{\partial^2 n(r)}{\partial r^2} = \left(\frac{dn}{dT}\right)_{eff} \frac{\partial^2 T(r)}{\partial r^2} \quad (10)$$

and therefore:

$$f_T \approx \frac{R^2}{2L\left(\frac{dn}{dT}\right)_{eff} \Delta T_{QSSR}}. \quad (11)$$

According to Fig. 5(b), the quasi-static RIC between the center and edges of the rod in the QSSR is $\Delta n_{QSSR} \sim 2.9\times10^{-5}$. Hence, the quasi-static focal lens induced by ΔT_{QSSR} is $f_T \approx 0.54$ m at λ = 1064 nm (Eq. (11)). This value is in good agreement with our experimental data $f_T \approx f_{qs} = 0.53 \pm 0.02$ m. The computed temperature modulation $\delta T(t)$ between the center and the edge of the Nd:YAG rod in the QSSR increases by ~ 0.13 K. During ~ 1 ms, it should result in a decrease of the thermal focal length of about $\frac{\delta f_T}{f_T} \approx \frac{\delta T(t)}{\Delta T_{QSSR}} = -3.2\%$ where δf_T accounts for the change of thermal focal lens. This is at variance with our experimental data which indicate an increase of the focal length by about $\frac{\delta f}{f_{qs}} \sim +10\%$ that lasts ~ 500 µs. We also perform a similar numerical simulation at λ = 532 nm (Fig. 4). As already mentioned, in this case we noticed that the central wavelength of the pump diode laser shifted by ~ 4 nm. Hence, we slightly lower the pump absorption coefficient (from 7.5% to 5.5%). Under this condition $\Delta T_{QSSR}^{532nm} \sim 3$ K whereas at maximum $\delta T(t) \sim 0.1$ K. Accordingly, and in good agreement with our experimental data, $f_T \approx f_{qs} \approx 0.74$ m. The temperature in the center of the Nd:YAG in the QSSR induces a

Optics EXPRESS

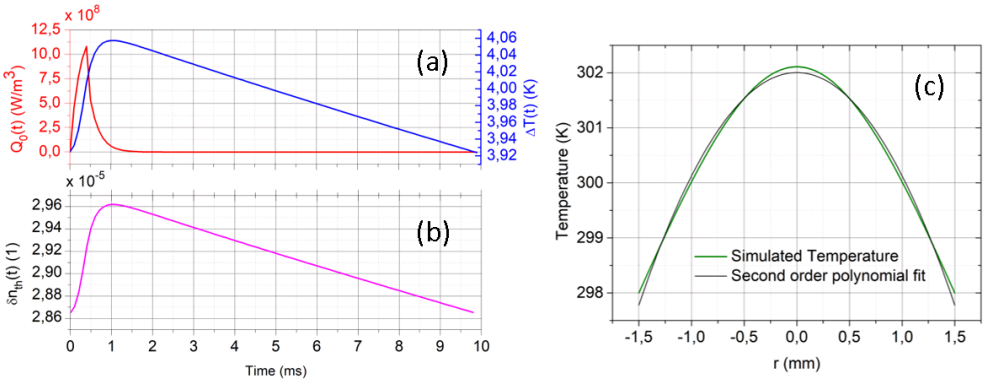

Fig. 5. (a) Temporal evolution of the heat generation coefficient $Q_0(t)$ (blue curve) and the change in temperature $\Delta T(t)$ (red curve) between the center and the edge of the rod during a pumping cycle. (b) Temporal evolution of the difference of refractive index between the center and the edge of the Nd:YAG rod (purple curve). (c) Computed quasi-steady state temperature distribution inside the rod (green curve). The black curve is a second order polynomial fit of the temperature distribution. The fitting function writes $T(r) = A_0 + A_2 r^2$ where $A_0 = 302.03$ K and $A_2 = -1.89$ K $\cdot$ m^{-2}.

Table 1. Parameters used to simulate the Nd:YAG rod heating

Element	Symbol	Value	Unit
Radius	R	1.5	mm
Length	L	7	cm
Density	ρ_{YAG}	4.55	$g.cm^{-3}$
Thermal conductivity	K_c	10.5	$W.(m.K)^{-1}$
Specific heat capacity	C_p	0.59	$J.(g.K)^{-1}$
Excited N_d^{3+} lifetime	τ	230	μs
Thermo-optic coefficient	$\left(\frac{dn}{dt}\right)_{eff}$	7.3×10^{-6}	K^{-1}
N_d^{3+} density in Nd:YAG doped at 1%	$N_{tot}^{1\%}$	1.38×10^{23}	cm^3
N_d^{3+} density in Nd:YAG doped at 0.6%	$N_{tot}^{0.6\%}$	8.28×10^{23}	cm^3
Laser period	T_{period}	10	ms
Equivalent size of the pump	σ_{pump}	0.75	mm
Pump diode central wavelength	λ_{pump}	808	nm
Laser source central wavelength	λ_{laser}	1064.5	nm
Quantum defect	η_h	24	%
Absorption efficiency coefficient at 808.0 nm	$\eta_{abs}^{808.0}$	7.5	%
Absorption efficiency coefficient at 803.7 nm	$\eta_{abs}^{803.7}$	5.5	%
Absorption coefficient at 808 nm	α	1.0626×10^3	m^{-1}

decrease of the focal length of the AM. However, whereas our simulation indicates $\frac{\delta T(t)}{\Delta T_{QSSR}} \sim -3\%$ at maximum, our data show that $\frac{\delta f}{f_{qs}} \sim -8\%$ at maximum. Besides, while experimentally the decrease of the focal length lasts 500 µs, our thermal simulation indicates that it should decrease during ~ 1 ms (see Fig. 4(b)). In conclusion, the model which only considers the heating of the Nd:YAG rod accounts well for the experimental quasi-static focal lens f_{qs}, but it fails to

Optics EXPRESS

correctly describe the modulation of f_{qs} in the QSSR. It is also worth mentioning that under slightly saturated absorption condition the kinetics of the thermal and excited population will be modified.

5. Modification of the Nd:YAG rod refractive index via the Nd^{3+} excited states population

The small modulation of the RIC of the AM in the QSSR has been previously reported [13–17]. Antipov et al. [13] have studied in detail the Nd:YAG RIC using a Jamin-Lebedev polarization interferometer. In this experiment, the Nd:YAG crystal was excited by pulsed laser diodes centered at λ_p = 808 nm and/or Nd:YAG laser pulses centered at λ_p = 266 nm. The RIC was measured using a probe beam centered at λ = 633 nm. Under their experimental conditions, they were able to demonstrate that the phase shift experienced by the probe beam exhibits two response times. In good agreement with the fitting of our experimental results (Fig. 4(b)), the shortest was ~ 238 ± 9 µs and the longest was ~ 6.0 ± 0.4 ms. They attributed these two time constants to the relaxation time of excited Nd^{3+} ions and the thermal response of the Nd:YAG rod. Accordingly, in addition to the thermal effect, they have added to the RIC the Nd:YAG change of polarizability contribution resulting from the Nd^{3+} excited state population. This contribution writes:

$$\delta n_e = \frac{2\pi F_L^2}{n_0}\Delta p(\nu) N_{ex}, \tag{12}$$

where $F_L = \frac{n_0^2+2}{3}$ is the Lorentz factor, n_0 the refractive index of the unexcited Nd:YAG rod, N_{ex} the density of excited Nd^{3+} ions and Δp the polarizability variation between the ground $^4I_{11/2}$ and the excited $^4F_{3/2}$ states at the probe wavelength. The polarizability $p(\nu)$ of the Nd:YAG rod at a frequency $\nu = \frac{c}{\lambda}$ is given by:

$$p_q(\nu) = \frac{\lambda n_0}{8\pi^2 F_L^2}\sum_i \frac{\sigma_{qi}\nu\Delta\nu_{qi}.(\nu_{qi}^2 - \nu^2)}{(\nu_{qi}^2 - \nu^2)^2 + \left(\nu\Delta\nu_{qi}\right)^2}, \tag{13}$$

where σ_{qi} is the absorption cross-section, ν_{qi} the frequency of the transition and $\Delta\nu_{qi}$ the linewidth of the transition between the q and i states. The parameters used to compute the polarizability of the Nd:YAG are summarized in the Table 2.

Table 2. Data used to compute the polarizability of the $^4F_{3/2} \rightarrow {}^4I_{9/2}$ transition [13].

Transition	λ (nm)	$\Delta\upsilon_i$ (cm^{-1})	σ_i. 10^{-19}(cm^2)	Transition	λ (nm)	$\Delta\upsilon_i$ (cm^{-1})	σ_i. 10^{-19}(cm^2)	Transition	λ (nm)	$\Delta\upsilon_i$ (cm^{-1})	σ_i. 10^{-19}(cm^2)
$^4F_{3/2}$ ↓ $^4I_{9/2}$				$^4F_{3/2}$ ↓ $^4I_{11/2}$	1052.1	4.5	0.95	$^4F_{3/2}$ ↓ $^4I_{13/2}$	1318.7	4.0	0.95
	869	13	0.41		1054.9	4.5	0.06		1320.4	4.6	0.23
	875.4	10	0.11		1061.5	4.6	2.50		1333.5	4.6	0.44
	879.2	18	0.13		1064.2	5.0	3.00		1335.1	3.3	0.54
	884.4	19	0.42		1064.4	4.2	1.45		1338.1	4.0	1.00
	885.8	19	0.35		1068.2	6.5	0.60		1341.9	6.0	0.36
	891.1	10	0.24		1073.7	4.6	1.65		1353.3	4.0	0.28
	893.4	31	0.05		1079.9	7	0.77		1357.2	4.0	0.73
	900.0	31	0.12		1105.5	11	0.16		1415.0	8.5	0.20
	938.6	10	0.48		1111.9	10.2	0.36		1427.1	7.0	0.08
	956.1	9	0.51		1115.8	10.6	0.42		1432.0	10.0	0.13
					1122.5	9.9	0.40		1444.4	9.0	0.28

According to equation (Eq. (13)) and far from any transition of the Nd^{3+} ions, the polarizability $p(\nu)$ of the Nd^{3+} remains almost constant. Moreover, we will neglect the small dispersion of

Optics EXPRESS

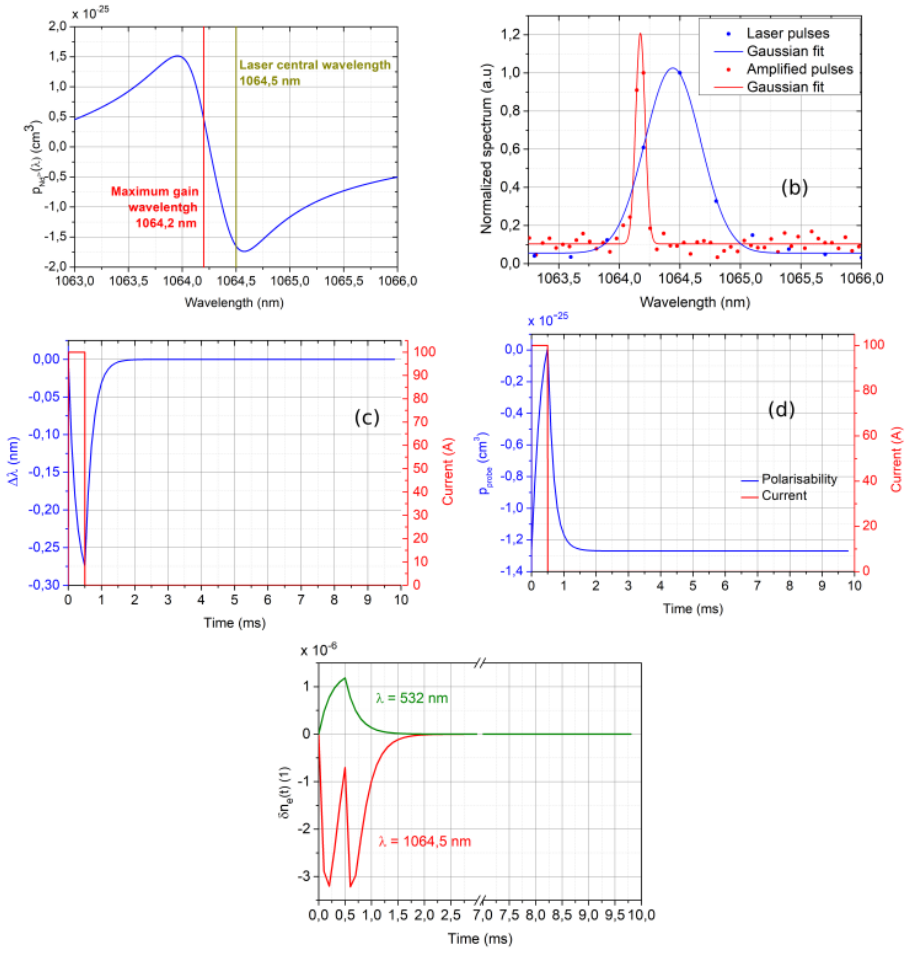

Fig. 6. (a) polarizability of the Nd^{3+} ions as a function of the wavelength. (b) Spectrum of the laser probe with (red curve) and without (blue curve) amplification in the Nd:YAG rod. (c) Temporal evolution of the laser diode electrical pulse (red curve) and simulation of the shift $\Delta\lambda$ experienced by the amplified probe pulse during a pumping cycle. (d) Temporal evolution of the laser diode electrical pulse (red curve) and the polarizability seen by the amplified laser pulse when its central wavelength shift (blue curve). (e) Temporal evolution of the RIC induced by the population of the Nd^{3+} excited state when the laser probe is centered at λ = 532 nm (green curve) and at λ = 1064.5 nm (red curve) during a pumping cycle.

the YAG matrix refractive index around λ_p = 1064 nm and λ_p = 532 nm. At λ_p = 532 nm or λ_p = 633 nm, the polarizability change is $\Delta p \sim 4\times10^{-26}$ cm^3 [13]. However, as soon as the probe pulse frequency is close to a transition of Nd^{3+} ions, the Nd:YAG rod polarizability rapidly changes. In Fig. 6(a), we plotted the Nd^{3+} polarizability variation around the transition between the $^4F_{3/2}$ and $^4I_{11/2}$ states centered at 1064.2 nm. It is worth noting that a small change of the probe wavelength from 1064.5 nm to 1064.0 nm results in a large change from $\Delta p \sim -1.7\times10^{-25}$ cm^3 to $\Delta p \sim 1.5\times10^{-25}$ cm^3 of the Nd^{3+} polarizability. This latter evolution is of importance for our experiment where the probe pulse central wavelength is initially about λ = 1064.5 nm. Upon its amplification in the Nd:YAG rod, the probe pulse central wavelength is slightly shifted towards the optimum amplification wavelength from 1064.5 nm to 1064.2 nm.

Optics EXPRESS

We highlight this phenomenon in Fig. 6(b), which displays the probe pulse spectrum with and without amplification in the AM. In the latter experiment, the probe pulse experiences a central wavelength shift $\Delta\lambda \sim$ 0.26 nm and a decrease of its spectral bandwidth. To account for this shift, we simulate the evolution of the gain at small signal, $g(\lambda)$, of the Nd:YAG versus the wavelength. Considering that the probe pulse spectrum is Gaussian in shape, centered at λ = 1064.5 nm with a half-width $\delta\lambda$ = 0.5 nm, we compute the amplified probe pulse central wavelength variation during the AM pumping (Fig. 6(c)). At the end of the pump pulse, which lasts 500 µs, the probe wavelength shift is about $\Delta\lambda \sim$ 0.26 nm. This induces the AM polarizability change (Fig. 6(d)). According to this figure, the maximum polarizability variation is $\sim 1.3\times10^{-25}$ cm^3. In Fig. 6(e), we plot the RIC temporal evolution between the center and the edge of the Nd:YAG rod during a pumping cycle. At $\lambda \sim$ 1064 nm, δn_e drops to $\sim -3\times10^{-6}$, whereas, it rises to $\sim 1\times10^{-6}$ at λ = 532 nm. In the simulations, the pump intensity distribution along the Nd:YAG rod diameter is Gaussian in shape and induces a Gaussian distribution of N_{ex}. The N_{ex} distribution is therefore well approximated by a second order polynomial, making it possible to directly infer the induced lens from δn_e.

6. Discussion

Taking into account the thermal and excited population contributions to the RIC, the Nd:YAG rod focal length evolution writes (Eq. (9)):

$$f(t) = -\frac{1}{2L\left(\left(\frac{\partial^2 n_T(t)}{\partial r^2}\right)_{r=0} + \left(\frac{\partial^2 n_e(t)}{\partial r^2}\right)_{r=0}\right)} \approx \frac{R^2}{2.L.(\Delta n_{QSSR} + \delta n_T(t) + \delta n_e(t))}, \tag{14}$$

where Δn_{QSSR}, $\delta n_T(t)$ and $\delta n_e(t)$ are the difference between the refractive index in the center and the edge of Nd:YAG rod, the temporal modulation resulting from the thermal and excited state population in QSSR, respectively. Accordingly, we computed the focal length evolution within the AM during a optical pumping cycle (Fig. 7). Experimental and numerical data are in good agreement. This indicates the thermal and excited population contributions to the RIC of Nd:YAG rod are well accounted. The thermal contribution is in fact almost independent on the probe wavelength and its kinetics is driven by the heat equation (Eq. (2)). It induces a quasi static lens f_{qs} and its temporal modulation induced by Δn_{QSSR} and $\delta n_T(t)$, respectively. On the contrary due to the Nd^{3+} polarizabilty variation, the excited state population contribution $\delta n_e(t)$ strongly depends on the probe wavelength (Fig. 6(e)) and its kinetics is driven by the Nd^{3+} excited population equation (Eq. (4)). It results in a temporal lens modulation induced by $\delta n_e(t)$.

When the probe pulse is centred at λ = 532 nm, Fig. 7(a) indicates the thermal and the excited state population contributions to the AM focal length add up. When the pump is on, both $\delta n_T(t)$ and $\delta n_e(t)$ increase. When the pump is off, $\delta n_T(t)$ still slowly increases during $\sim$ 500 µs (Fig. 5(b)) whereas $\delta n_e(t)$ more rapidly decreases according to the relaxation of N_{ex} (Fig. 6(e)). In consequence, the AM focal length decreases rapidly during $\sim$ 500 µs. Afterwards, the AM focal length decreases more slowly due to heat diffusion in the AM.

When the probe pulse is centred at λ = 1064.5 nm, Fig. 7(b)-(c)) indicate a very different behavior. At this wavelength, the Nd^{3+} polarizability contribution to δn_e is large and negative. Since $\delta n_e \sim -3\delta n_T$ at maximum, we simplify the discussion and assume that the behavior displayed these figures mainly results from $\delta n_e(t) + \Delta n_{QSSR}$ which kinetics is displayed in Fig. 6(e). When the pump is switched on (resp. off), N_{ex} rapidly increases (resp. decreases), $\delta n_e(t) + \Delta n_{QSSR}$ decreases (resp. increase) inducing an increase (resp decrease) of the AM focal length. As N_{ex} further increases, the AM gain increases resulting in a shift backward (resp. forward) of the probe central wavelength. The latter experiences a reduction (resp. an increase) of the Nd^{3+} polarizability (Fig. 6(d)) which induces an increase (resp. decrease) of $\delta n_e(t) + \Delta n_{QSSR}$. Hence,

Optics EXPRESS

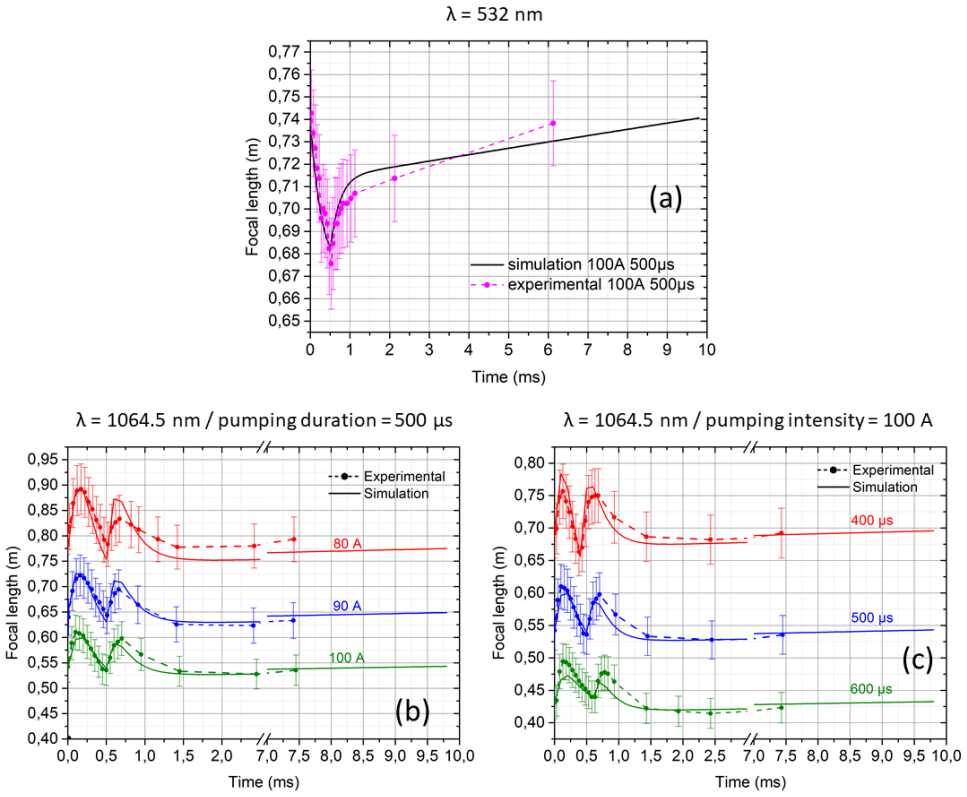

Fig. 7. Comparison between the simulated and the experimental data. (a) For a probe pulse centered at $\lambda = 532$ nm and a pump laser diode current of $I = 100$ A and a duration $\tau_{pump} = 500$ µs. (b) For a probe pulse centered at $\lambda = 1064.5$ nm and a pump laser diode pulse with $\tau_{pump} = 500$ µs duration, with different electrical currents. (c) For a probe pulse centered at $\lambda = 1064.5$ nm and pump laser diode electrical pulse of different durations with a current $I = 100$ A.

the AM focal length decreases (resp. increases). As soon as the pump pulse is switched off, the reverse process takes place.

7. Conclusions

In summary, we evaluated the focusing effect induced in a Nd:YAG rod amplifier. The experiment we built makes it possible to measure at different wavelengths the temporal evolution of the focal lens induced in a AM rod submitted to periodic pump pulses of a few hundred microseconds. We also develop a model which well accounts for the evolution recorded experimentally. This model is valid in the unsaturated regime and low pump duty cycle. These experiments and the simulations indicate that two different mechanisms are responsible for a quasi-static focal lens f_{qs} and its periodic modulation $\delta f(t)$. When the AM is optically pumped, its temperature increases and a quasi-static temperature gradient ΔT_{QSSR} is induced along the rod diameter. It results in a gradient of refractive index Δn_{QSSR} which makes the AM acts as a lens with focal length f_{qs}. It is the latter contribution which is usually compensated in a conventional amplifier system. However, when the steady state regime is established, a small periodic temperature modulation $\delta T(t)$ of the AM remains. The latter induces a small periodic modulation of thermal AM focal

Optics EXPRESS

length $\delta f(t)$. Besides the thermal effect, we have shown that another phenomenon related to the Nd^{3+} excited state population must be added. When the probe pulse wavelength is far from any Nd^{3+} resonances, for instance at $\lambda = 532$ nm, these two contributions add and result in a periodic modulation of f_{qs}. The different temporal evolutions of these two phenomena make it possible to easily discriminate them. When the probe beam wavelength is at $\lambda = 1064.5$ nm, close to a resonance of the Nd^{3+}, it is amplified in the AM and experiences a drastic change in AM polarizability induced by the population excited state. This latter phenomenon results from the probe pulse amplification which induces a shift of its central wavelength which in turn results in an original evolution of periodic modulations of the f_{qs}. Our experiment clearly evidences this phenomenon and indicates that this effect may partly compensate for the thermal lens effect. This effect should be more pronounced reducing the quasi steady steady state lens. This can be achieved by reducing the pump repetition rate while keeping the pump peak power constant.

Funding. Conseil Régional Aquitaine; Agence Nationale de la Recherche (LAMA ANR-18-ASMA-0004-01).

Disclosures. The authors declare no conflicts of interest.

Data availability. Data underlying the results presented in this paper are not publicly available at this time but may be obtained from the authors upon reasonable request.

References

1. T. Kawasaki, V. Yahia, and T. Taira, "100 Hz operation in 10 PW/sr·cm^2 class Nd:YAG Micro-MOPA," Opt. Express **27**(14), 19555–19561 (2019).
2. J. Ding, G. Yu, R. Zheng, J. Zhou, X. Zhu, W. Duan, C. Fang, and W. Wei, "A compact, high-power single-frequency laser based on Nd:YAG slab amplifier," Opt. Commun. **464**, 125534 (2020).
3. M. Xu, Y. Guo, J. Su, and H. Lu, "125 W single-frequency CW Nd:YVO_4 laser based on two-stage dual-end-pumped master-oscillator power amplifiers," Laser Phys. Lett. **16**(3), 036201 (2019).
4. Y. Jiang, J. Yang, P. Li, H. Si, X. Fu, and Q. Liu, "High energy LiDAR source for long distance, high resolution range imaging," Microw. Opt. Technol. Lett. **62**(12), 3655–3661 (2020).
5. A. Kornev, R. Balmashnov, I. Kuchma, A. Davtian, and D. Oborotov, "0.43 J/100 ps Nd: YAG laser with adaptive compensation of thermally induced lens," Opt. Lett. **43**(18), 4394–4397 (2018).
6. Y. Zhang, Y. Qi, S. Yang, N. Luan, Z. Bai, J. Ding, Y. Wang, and Z. Lu, "High pulse energy, narrow-linewidth all-fiber 1064 nm picosecond master oscillator power amplifier system," Opt. Laser Technol. **147**, 107636 (2022).
7. W. Koechner, "Thermal lensing in a Nd:YAG laser rod," Appl. Opt. **9**(11), 2548–2553 (1970).
8. S. Chénais, F. Druon, S. Forget, F. Balembois, and P. Georges, "On thermal effects in solid-state lasers: The case of ytterbium-doped materials," Prog. Quantum Electron. **30**(4), 89–153 (2006).
9. S. Chenais, "Nouveaux matériaux laser dopés à l'ytterbium: performances en pompage par diode et étude des effets thermiques," Ph.D. thesis, Université Paris Sud-Paris XI (2002).
10. X. Peng, L. Xu, and A. K. Asundi, "Thermal lensing effects for diode-end-pumped Nd:YVO_4 and Nd: YAG lasers," Opt. Eng. **43**(10), 2454–2461 (2004).
11. K. Yumashev, A. Zakharova, and P. Loiko, "Photo-elastic effect, thermal lensing and depolarization in a-cut tetragonal laser crystals," Laser Phys. **26**(6), 065002 (2016).
12. P. Shang, M. Wu, S. Wang, D. Cai, and B. bin Li, "Thermal lens Q-switched 1064 nm Nd:YAG laser," Opt. Commun. **507**, 127676 (2022).
13. O. L. Antipov, O. Eremeikin, and A. P. Savikin, "Interferometric study of electronic changes in the refractive index of a Nd:YAG laser crystal caused by intense pumping," Quantum Electron. **33**(10), 861–868 (2003).
14. E. Anashkina and O. Antipov, "Electronic (population) lensing versus thermal lensing in Yb:YAG and Nd:YAG laser rods and disks," J. Opt. Soc. Am. B **27**(3), 363–369 (2010).
15. L. Freitas, C. Jacinto, A. Rodenas, D. Jaque, and T. Catunda, "Time-resolved study electronic and thermal contributions to the nonlinear refractive index of Nd^{3+}:SBN laser crystals," J. Lumin. **128**(5-6), 1013–1015 (2008).
16. C. Jacinto, D. N. Messias, A. A. Andrade, S. Lima, M. J. V. Bell, S. L. Oliveira, M. L. Baesso, L. A. d. O. Nunes, and T. Catunda, "Refractive index changes in solid-state laser materials," in *Topical Problems of Nonlinear Wave Physics*, vol. 5975 (SPIE, 2006), pp. 175–187.
17. A. Andrade, E. Tenorio, T. Catunda, M. Baesso, A. Cassanho, and H. Jenssen, "Discrimination between electronic and thermal contributions to the nonlinear refractive index of $SrAlF_5$:Cr^{3+}," J. Opt. Soc. Am. B **16**(3), 395–400 (1999).
18. D. N. Messias, T. Catunda, J. D. Myers, and M. J. Myers, "Nonlinear electronic line shape determination in Yb^{3+}-doped phosphate glass," Opt. Lett. **32**(6), 665–667 (2007).
19. R. Moncorgé, O. Eremeykin, J. Doualan, and O. Antipov, "Origin of athermal refractive index changes observed in Yb^{3+} doped YAG and KGW," Opt. Commun. **281**(9), 2526–2530 (2008).

Optics EXPRESS

20. O. L. Antipov, D. V. Bredikhin, O. N. Eremeykin, A. P. Savikin, E. V. Ivakin, and A. V. Sukhadolau, "Electronic mechanism for refractive-index changes in intensively pumped Yb:YAG laser crystals," Opt. Lett. **31**(6), 763–765 (2006).
21. O. Antipov, O. Eremeykin, A. Savikin, V. Vorob'ev, D. Bredikhin, and M. Kuznetsov, "Electronic changes of refractive index in intensively pumped Nd:YAG laser crystals," IEEE J. Quantum Electron. **39**(7), 910–918 (2003).
22. N. Passilly, E. Haouas, V. Ménard, R. Moncorgé, and K. Aït-Ameur, "Population lensing effect in Cr:LiSAF probed by Z-scan technique," Opt. Commun. **260**(2), 703–707 (2006).
23. R. C. Powell, S. A. Payne, L. L. Chase, and G. D. Wilke, "Index-of-refraction change in optically pumped solid-state laser materials," Opt. Lett. **14**(21), 1204–1206 (1989).
24. J. Margerie, R. Moncorgé, and P. Nagtegaele, "Spectroscopic investigation of variations in the refractive index of a Nd:YAG laser crystal: Experiments and crystal-field calculations," Phys. Rev. B **74**(23), 235108 (2006).
25. H. Danielmeyer, M. Blätte, and P. Balmer, "Fluorescence quenching in Nd:YAG," Appl. Phys. **1**(5), 269–274 (1973).
26. A. E. Siegman, *Lasers* (University Science Books, 1986).
27. B. Comaskey, B. Moran, G. Albrecht, and R. Beach, "C[illegible]erization of the heat loading of ~~nd-doped yag, yos, ylf, and ggg~~ excited at diode pumping wavelengths," IEEE J. Quantum Electron. **31**(7), 1261–1264 (1995).